RSC Advances

PAPER

View Article Online
View Journal | View Issue

Cite this: *RSC Adv.*, 2024, **14**, 32206

Supramolecular motifs formed by CH_3/Cl-substituted arene groups: evidence for structural differences in thiophosphoramides and similarities in their complexes†

Saeed Hosseinpoor, [a] Mehrdad Pourayoubi, *[a] Eliška Zmeškalová [b] and Morgane Poupon[b]

Differences/similarities of supramolecular motifs are discussed in two new thiophosphoramide structures and their Ni molecular complexes: $(C_2H_5O)_2P(S)(NHC(S)NHCH_2C_6H_4X)$ and $[\{(C_2H_5O)_2P(S)(NC(S)NHCH_2C_6H_4X)\}_2Ni]$ (X = Cl/CH_3 **I**/**II** and **III**/**IV**). The structures have equal numbers of donor/acceptor sites contributing to classical hydrogen bonds (PS/CS and 2 × NH in ligands and 2 × PS and 2 × NH in the complexes). However, these donor and acceptor sites contribute to inter/intramolecular hydrogen bonding in ligands and intramolecular hydrogen bonding in complexes. In the supramolecular assemblies of the ligands, the classic hydrogen bonds (N–H···S=C) are restricted in dimer synthons, and the weaker interactions (formed by Cl/CH_3 substituents) compete against each other. In the complexes, despite the lack of classic intermolecular hydrogen bond, numerous weak interactions, *e.g.*, C–H···Y (Y = S, O, Ni, N, and π), contribute to the molecular assemblies, which do not include the participation of Cl/CH_3. Thus, different packing features of ligands, but similar in complexes are observed. Each ligand and the associated complex show nearly equal supramolecular motifs in the slice of the substituted benzyl groups, related to the formation of C–H···Cl/π···π for the 4-Cl-$C_6H_4CH_2$ groups in **I**/**III** and C–H···π for the 4-CH_3-$C_6H_4CH_2$ groups in **II**/**IV**. The repeatabilities of the motifs made by 4-Cl-$C_6H_4CH_2$/4-CH_3-$C_6H_4CH_2$ were checked by surveying 142/844 structures with 178/1482 segments in the CSD, which show that 17% and 12% of the structures exhibited similarities with the title structures. The methods X-ray crystallography, 2D fingerprint plots, electrostatic potential surfaces, QTAIM, and energy framework calculations were applied to present the discussion.

Received 20th July 2024
Accepted 25th September 2024

DOI: 10.1039/d4ra05281a

rsc.li/rsc-advances

Introduction

The prediction and design of crystalline structures have been a topic of interest, due to various applications in material sciences and pharmaceutics.[1–4] In this context, strong to moderate interactions, notably hydrogen bonds, play a significant role in forming molecular assemblies and are extensively addressed.[3,5–7] Although weak interactions often have less impact on the formation of supramolecular assemblies, their role is still questionable, and there are reports on the study of such interactions in molecular/ionic crystal structures[5,8] and macromolecule materials.[9,10]

The importance of weak interactions can become clearer when two almost the same molecules with just a difference in the substituent (influential for weak interactions) form two crystal structures with different packing features.[11,12] In organic compounds, Cl/CH_3 units—which have about the same volume—are frequently utilized as substituents. Their disparate electrical characteristics lead to different actions as donor/acceptor sites in contacts and to form different molecular assemblies. The electron density of chlorine, bonded to one other atom, is anisotropically distributed, resulting in the formation of (i) a negative belt orthogonal to the covalent bond (a possible electron donor site) and (ii) a σ-hole upward of the chlorine bond with lower electron density and generally positive electrostatic potential (a possible electron acceptor site).[5,13]

However, the expected behavior of organic chlorine is its hydrogen acceptor capability in weak hydrogen bonds. Methyl groups, with positive electrostatic potential on their hydrogens, usually take part in weak hydrogen bonds and dihydrogen

[a]*Department of Chemistry, Faculty of Science, Ferdowsi University of Mashhad, Mashhad, Iran. E-mail: pourayoubi@um.ac.ir*

[b]*Institute of Physics of the Czech Academy of Sciences, Na Slovance 2, Prague 8, 182 21, Czech Republic*

† Electronic supplementary information (ESI) available. CCDC 2311920–2311923. For ESI and crystallographic data in CIF or other electronic format see DOI: https://doi.org/10.1039/d4ra05281a

interactions. Nevertheless, a negative region on the associated carbon atom was calculated, where it is bonded to an electropositive atom, proposing the potential electron donor behavior.[14,15] In fact, the electron density around methyl is practically distributed in opposition to chlorine.

In addition to direct interactions of substituents, their influence on the electrostatic potential of neighboring groups can impact the molecular assembly. Regarding the substitutions of the aryl groups, Wheeler showed the through-space effect of substituents on the electrostatic potential,[16] although he explained that the main effect of substituents is due to their direct and local interaction.[17,18]

Some researchers show that exchanging non-polar substituents with the same sizes in molecules[19] (*e.g.* Cl/CH_3) or even with different sizes[20] (*e.g.* CF_3/CH_3) may cause the production of isostructures. Further research showed that in some cases, the directional interactions of Cl atoms may alter the structure.[21] An old CSD study indicated that about 30% of the crystal structures with Cl/CH_3-substitution that had been documented up to that time were isostructure.[22] Earlier investigations affirm the isostructurality in Cl/CH_3-exchanged crystal structures, in which interactions with no contribution of the Cl atom dominate.[23–27] In some structures where the DH···Cl (D = hydrogen donor atom) and Cl···Cl interactions are dominant with respect to other weak interactions, the structures are changed by exchanging the Cl atom with the CH_3 group.[24,28,29] Moreover, there are examples of structural similarity of hydrogen bond pattern, based on stronger interactions, but with differences in crystal packing related to the contribution of Cl/CH_3.[30] Nonetheless, the prediction of the possible isostructurality is challenging, and it is still up for discussion how weak to moderate interactions play a role in discriminating or not in structures with exchanged methyl and chloro substituents.

The $(R^1O)_2P(S)(NHC(S)R^2)$ thiourea-based thiophosphoramides (R^1 = aryl/alkyl, and R^2 = amine groups) are studied in complexation processes,[31,32] manufacturing of antibacterial agents,[33,34] membranes,[35] as sulfide donor precursors in the fabrication of photoluminescence thin-films,[36,37] and in the concepts related to crystal engineering.[32,38,39]

Some attempts have been made to look into the structural features of the thiophosphoramide family affected by the methyl and chlorine substituents, individually. However, the comparison of motifs and interactions created by chlorine/methyl substituted aryl groups and their effects on supramolecular assemblies is limited to a pair of Hg complexes.[40] Herein, we report on two new thiourea-based thiophosphoramide structures and their nickel complexes, including CH_3/Cl substituents attached to an arene ring (**I–IV**, Chart 1). The differences between these structures are probed by closely looking at the crystal structures using computational methods. The role of weak interactions is examined in the effectiveness of Cl/CH_3 exchange on structural changes. Additionally, the structures with 4-Cl-$C_6H_4CH_2$ and 4-CH_3-$C_6H_4CH_2$ fragments were retrieved from the Cambridge Structural Database to find the probability of the creation of the aryl···aryl motifs similar to **I/III** and **II/IV**.

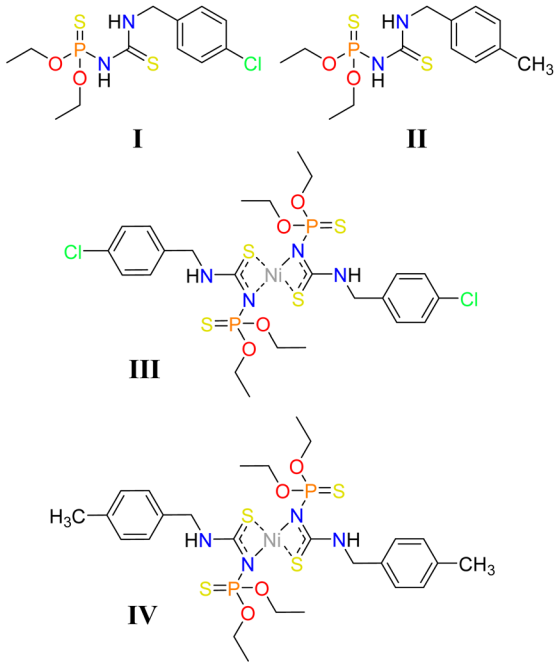

Chart 1 Structural formulas of I–IV.

Experimental and theoretical methods

Diffraction data were collected on a Rigaku/Oxford Diffraction diffractometer using Cu Kα radiation at 95 K (**I**) and 120 K (**II–IV**). The data were registered with an Atlas S2 CCD area detector. CrysAlis PRO[41] was used to control the experiment and process data. Shelxt[42] was used for the structure solution, and Jana2020 [43] was used to refine and finalize the structure model. The structures were solved by the direct method and refined by the full-matrix least-squares method on F^2. All non-hydrogen atoms were refined anisotropically, and the hydrogen atoms were all located on a difference-Fourier map, but those attached to carbon atoms were repositioned geometrically. The H atoms were initially refined with soft restraints on the bond lengths and angles to regularize their geometry (C–H in the range 0.93–0.98 Å, N–H in the range 0.86–0.89 Å and $U_{iso}(H)$ in the range 1.2–1.5 times U_{eq} of the parent atom), after which the positions were refined with riding constraints.

X-ray crystallographic parameters of **I–IV** are gathered in Table 1, and selected bond lengths and angles and hydrogen bond parameters are given in Tables S1–S5.† The molecular structures are represented in Fig. S1.†

All the chemical substances utilized in this investigation were procured from commercially available sources and employed in their original state. ^1H, $^{13}C\{^1H\}$, and $^{31}P\{^1H\}$ NMR spectra were recorded using a Bruker Avance III 300 MHz spectrometer. As external standards, chemical shifts were determined relative to TMS for ^1H and ^{13}C and 85% H_3PO_4 for ^{31}P. IR spectra were recorded on a Buck 500 Scientific spectrometer using KBr pellets. The mass spectra were recorded with a Varian Mat CH-7 spectrometer at 70 eV.

Table 1 Crystallographic parameters of the structures I–IV

	I	II	III	IV
Chemical formula	$C_{12}H_{18}ClN_2O_2PS_2$	$C_{13}H_{21}N_2O_2PS_2$	$C_{12}H_{17}ClN_2Ni_{0.50}O_2PS_2$	$C_{13}H_{20}N_2Ni_{0.50}O_2PS_2$
M_r	352.85	332.43	381.19	360.77
Crystal system, space group	Triclinic, $P\bar{1}$	Triclinic, $P\bar{1}$	Triclinic, $P\bar{1}$	Triclinic, $P\bar{1}$
Temperature (K)	95	120	120	120
a, b, c (Å)	7.6290 (1), 7.6702 (1), 14.1025 (4)	5.8046 (2), 10.7878 (2), 13.3907 (3)	7.8502 (2), 10.1868 (4), 11.6914 (4)	8.2171 (3), 9.9942 (4), 11.1612 (4)
α, β, γ (°)	94.2128 (19), 99.531 (2), 98.0165 (16)	81.0002 (18), 83.334 (2), 89.276 (2)	113.275 (3), 97.462 (3), 97.123 (3)	113.611 (3), 93.655 (3), 92.926 (3)
V (Å^3)	801.93 (3)	822.58 (4)	835.66 (5)	835.21 (6)
Z	2	2	2	2
μ (mm^{-1})	5.51	3.88	5.86	4.39
Crystal size (mm)	0.49 × 0.27 × 0.14	0.79 × 0.55 × 0.38	0.31 × 0.27 × 0.12	0.76 × 0.28 × 0.22
T_{min}, T_{max}	0.11, 0.46	0.10, 0.23	0.15, 0.49	0.03, 0.38
No. of measured, independent, and observed [$I > 2.0\sigma(I)$] reflections	11 539, 3210, 3153	13 323, 2929, 2793	12 744, 2996, 2716	13 759, 2985, 2692
R_{int}	0.023	0.038	0.096	0.068
$(\sin\theta/\lambda)_{max}$ (Å^{-1})	0.624	0.600	0.600	0.600
$R[F^2 > 2\sigma(F^2)]$	0.026	0.031	0.050	0.045
w$R(F^2)$	0.071	0.097	0.141	0.139
S	0.97	1.04	1.00	0.99
No. of reflections	3210	2929	2996	2985
No. of parameters	182	190	188	187
$\Delta\rho_{max}$, $\Delta\rho_{min}$ (e Å^{-3})	0.54, −0.28	0.36, −0.37	0.76, −0.81	0.64, −0.91

The molecular electrostatic potential (ESP) surfaces were calculated using the Gaussian 09 software[44] at the B3LYP/cc-pVDZ level of theory, for molecules extracted from crystal structures after neutron-normalization of hydrogen positions.

Crystal lattice energies of structures **I** and **II** were calculated using CrystalExplorer 21.5 with the CE-B3LYP method and 6-31G(d,p) basis set.[45] In this approach, the interaction energies of a molecule with the first sphere of the neighboring molecules are computed, and the effects of the further molecules on the lattice energy are ignored. The interaction energies (E_{tot}) are calculated using the equation:

$$E_{tot} = k_{ele}E_{ele} + k_{pol}E_{pol} + k_{dis}E_{dis} + k_{rep}E_{rep}$$

where the k values are scale factors (given in Table S6†), and E_{ele}, E_{pol}, E_{dis}, and E_{rep} are electrostatic, polarization, dispersion, and repulsion energies. These energy components are calculated individually rather than breaking down a much larger total energy.[46] Crystal lattice energies (E_{latt}) are calculated using $E_{latt} = \frac{1}{2}\sum NE_{tot}$ formula,[47] in which N is the number of molecular pairs in the molecular shell, and E_{tot} is the total energy of each molecular pair. Crystal lattice energies, interaction energies of molecular pairs, and their components (electrostatic, dispersion, polarization, and repulsion) are given in Tables S7 and S8.†

Intermolecular interactions of molecular pairs with the most prominent energies in the crystal structure were studied using the QTAIM method.[48] In structures **I** and **II**, the molecular pairs with total interaction energies ≤ −15 kJ mol^{-1} (obtained from crystal lattice energy calculations) were selected. The wavefunction files were obtained using Gaussian 09 software[44] with the D3-B3LYP/cc-pVDZ level of theory, and the QTAIM diagrams were plotted with the MultiWFN program package.[49] Selected topological parameters including potential energy density ($V(r)$), kinetic energy density ($G(r)$), total energy density ($H(r)$), total electronic density ($\rho(r)$), and its corresponding Laplacian ($\nabla^2\rho(r)$) at bond critical points (BCPs) are given in Table 2. The $V(r)$ values can be applied in the formula $E = V(r)/2$ for estimating the hydrogen bond strength of molecular systems in the gas phase.[50] In the crystal structures, reporting the interaction energy values obtained from this estimation can be misguiding due to some observed deviations from the results of other computational methods.[51] Nevertheless, the $V(r)$ values can still be utilized as a criterion for the approximate comparison of the interaction strengths that are employed in this study. The $\rho(r)$ is another parameter that is used for approximate comparison of the interaction strength.[52] Based on Koch–Popelier criteria if the $\rho(r)$ value at a BCP of a CH···X contact ranges at 0.002–0.035 a.u. a hydrogen bond is established.[53]

The 2D fingerprint plot represents the distance of each point on the Hirshfeld surface to the nearest internal atom (d_i) and external atom (d_e). Accordingly, the term $d_i + d_e$ can be used as a criterion for estimating interaction strengths. The fragment patches of the generated Hirshfeld surface show the regions in contact with neighbor molecules and their area.

Synthesis and crystallization

Preparation of $(C_2H_5O)_2P(S)(NHC(S)NHCH_2C_6H_4$-4-Cl) (I) and $(C_2H_5O)_2P(S)(NHC(S)NHCH_2C_6H_4$-4-$CH_3)$ (II). A solution of *O*,*O*-diethyl chlorothiophosphate in anhydrous acetonitrile was

Table 2 Topological parameters for BCPs of structures **I–IV** with $V(r) < -0.0010$ a.u

Pair code	Interaction	$\rho(r)$	$\nabla^2\rho(r)$	$G(r)$	$V(r)$	$H(r)$
Intramolecular (**I**)	NH···S=P	0.0194	0.0473	0.0111	−0.0104	0.0007
Ia	NH···S=C	0.0224	0.0473	0.0115	−0.0112	0.0003
	CH···S=C	0.0061	0.0185	0.0039	−0.0031	0.0008
Ib	CH···O	0.0089	0.0274	0.0065	−0.0062	0.0003
Ic	CH···S=C	0.0048	0.0150	0.0030	−0.0022	0.0008
	CH···N	0.0063	0.0215	0.0045	−0.0037	0.0008
	CH···O	0.0041	0.0180	0.0035	−0.0025	0.0010
Id	CH···S=P	0.0060	0.0152	0.0033	−0.0028	0.0005
	CH···N	0.0044	0.0165	0.0033	−0.0024	0.0009
	CH···S=C	0.0043	0.0128	0.0026	−0.0020	0.0006
	CH···S=C	0.0042	0.0127	0.0026	−0.0020	0.0006
	CH···π	0.0066	0.0200	0.0042	−0.0033	0.0009
	NH···Cl	0.0038	0.0137	0.0028	−0.0021	0.0007
	CH···Cl	0.0048	0.0156	0.0031	−0.0022	0.0009
	CH···Cl	0.0050	0.0162	0.0033	−0.0025	0.0008
	CH···HC	0.0048	0.0177	0.0035	−0.0026	0.0009
Ie	CH···S=C	0.0035	0.0112	0.0022	−0.0015	0.0007
	CH···S=C	0.0041	0.0114	0.0023	−0.0018	0.0005
	CH···S=P	0.0077	0.0211	0.0046	−0.0038	0.0008
If	π···π	0.0052	0.0122	0.0026	−0.0022	0.0004
	CH···Cl	0.0064	0.0219	0.0044	−0.0034	0.0010
	C(π)···Cl	0.0055	0.0161	0.0033	−0.0027	0.0006
Ig	CH···S=P	0.0056	0.0173	0.0035	−0.0026	0.0009
	CH···HC	0.0047	0.0162	0.0033	−0.0025	0.0008
Intramolecular (**II**)	NH···S=P	0.0202	0.0474	0.0113	−0.0108	0.0005
IIa	NH···S=C	0.0219	0.0462	0.0112	−0.0109	0.0003
	CH···S=C	0.0061	0.0206	0.0041	−0.0032	0.0009
	CH···S=C	0.0039	0.0128	0.0025	−0.0018	0.0007
IIb	CH···S=C	0.0037	0.0102	0.0021	−0.0016	0.0005
	O···S=P	0.0033	0.0117	0.0023	−0.0018	0.0005
	N···S=P	0.0044	0.0120	0.0026	−0.0023	0.0003
	CH···O	0.0101	0.0311	0.0075	−0.0073	0.0002
	CH···HC	0.0033	0.0129	0.0024	−0.0015	0.0009
	CH···HC	0.0030	0.0119	0.0021	−0.0013	0.0008
	CH···HC	0.0040	0.0143	0.0026	−0.0015	0.0011
	CH···HC	0.0040	0.0149	0.0028	−0.0019	0.0009
IIc	CH···S=P	0.0091	0.0247	0.0054	−0.0047	0.0007
	NH···π	0.0050	0.0174	0.0034	−0.0025	0.0009
	CH···π	0.0073	0.0223	0.0047	−0.0038	0.0009
	π···π	0.0043	0.0109	0.0023	−0.0019	0.0004
IId	CH···S=C	0.0066	0.0173	0.0037	−0.0031	0.0006
	CH···HC	0.0032	0.0122	0.0022	−0.0013	0.0009
IIe	CH···S=P	0.0040	0.0112	0.0023	−0.0017	0.0006
	CH···π	0.0049	0.0162	0.0032	−0.0025	0.0007
	CH···π	0.0040	0.0126	0.0026	−0.0020	0.0006
IIf	CH···HC	0.0042	0.0173	0.0031	−0.0020	0.0011
	CH···HC	0.0045	0.0180	0.0034	−0.0022	0.0012
Intramolecular (**III**)	NH···S=P	0.0201	0.0536	0.0128	−0.0122	0.0006
IIIa	CH···O	0.0050	0.0193	0.0040	−0.0032	0.0008
	CH···S=P	0.0068	0.0211	0.0044	−0.0035	0.0009
	CH···N	0.0049	0.0166	0.0035	−0.0029	0.0006
	CH···π	0.0044	0.0142	0.0028	−0.0022	0.0006
	CH···Ni	0.0062	0.0187	0.0039	−0.0032	0.0007
IIIb	CH···S=P	0.0078	0.0227	0.0049	−0.0041	0.0008
IIIc	CH···S=P	0.0040	0.0128	0.0025	−0.0017	0.0008
	CH···HC	0.0034	0.0140	0.0026	−0.0017	0.0009
	CH···HC	0.0024	0.0123	0.0022	−0.0013	0.0009
IIId	CH···S=P	0.0042	0.0136	0.0027	−0.0019	0.0008
	CH···Cl	0.0038	0.0125	0.0025	−0.0020	0.0005
	Cl···S	0.0048	0.0122	0.0026	−0.0022	0.0004
IIIe	CH···S–C	0.0050	0.0152	0.0031	−0.0024	0.0007
	CH···O	0.0028	0.0132	0.0024	−0.0015	0.0009
	CH···HC	0.0045	0.0182	0.0034	−0.0023	0.0011

Table 2 (*Contd.*)

Pair code	Interaction	$\rho(r)$	$\nabla^2\rho(r)$	$G(r)$	$V(r)$	$H(r)$
	CH···HC	0.0035	0.0142	0.0027	−0.0018	0.0009
IIIf	CH···Cl	0.0050	0.0162	0.0033	−0.0026	0.0007
	π···π	0.0048	0.0116	0.0025	−0.0021	0.0004
Intramolecular (**IV**)	NH···S=P	0.0183	0.0502	0.0118	−0.0111	0.0007
IVa	CH···O	0.0066	0.0227	0.0051	−0.0045	0.0006
	CH···O	0.0032	0.0133	0.0026	−0.0018	0.0008
	CH···S=P	0.0055	0.0187	0.0036	−0.0025	0.0011
	CH···π	0.0066	0.0217	0.0045	−0.0035	0.0010
	CH···Ni	0.0057	0.0184	0.0037	−0.0027	0.0010
IVb	CH···S=P	0.0042	0.0119	0.0024	−0.0017	0.0007
	CH···S=P	0.0041	0.0129	0.0025	−0.0018	0.0007
IVc	CH···HC	0.0034	0.0166	0.0028	−0.0015	0.0013
IVd	CH···S=P	0.0044	0.0123	0.0025	−0.0020	0.0005
	CH···S=P	0.0041	0.0128	0.0025	−0.0018	0.0007
IVe	CH···O	0.0020	0.0092	0.0016	−0.0010	0.0006
	CH···HC	0.0045	0.0211	0.0037	−0.0022	0.0015
IVf	CH···S–C	0.0033	0.0095	0.0019	−0.0014	0.0005
	CH···π	0.0032	0.0090	0.0018	−0.0014	0.0004

treated under vigorous stirring with potassium thiocyanate (1 : 1 mole ratio) for 18 hours. The potassium chloride salt was filtered off, and the filtrate was reacted with 4-chlorobenzylamine for **I** or 4-methyl benzylamine for **II** (1 : 1 mole ratio). After 4 hours, the solution was filtered off and left for slow evaporation. The obtained crystals, suitable for X-ray analysis, were separated, washed with acetonitrile, and dried.

I: m.p.: 84 °C. IR (KBr disc, ν, cm^{-1}): 3258, 3099, 2920, 1552, 1492, 1417, 1330, 1284, 1181, 1098, 1026, 879, 806. MS (70 eV, EI): m/z (%) = 353 (2) $[M + 1]^+$, 352 (22) $[M]^+$, 292 (23) $[M–2C_2H_6]^+$, 259 (34) $[M–2C_2H_5OH–1]^+$, 139 (98) $[C_7H_6ClN]^+$, 121 (97) $[CNPS_2]^+$, 77 (65) $[C_6H_5]^+$, 29 (100) $[C_2H_5]^+$. $^{31}P\{^1H\}$ NMR (121 MHz, DMSO-d_6): δ (ppm) = 60.57 (s). ^1H NMR (301 MHz, DMSO-d_6): δ (ppm) = 9.33 (s, 1H), 8.55 (t, $^3J_{H–H}$ = 5.6 Hz, 1H), 7.43 (d, $^3J_{H–H}$ = 8.5 Hz, 2H), 7.34 (d, $^3J_{H–H}$ = 8.5 Hz, 2H), 4.70 (apparent d, J = 5.6 Hz, 2H), 4.12 (m, 4H), 1.27 (*t*, $^3J_{H–H}$ = 7.0 Hz, 6H). $^{13}C\{^1H\}$ NMR (75 MHz, DMSO-d_6): δ (ppm) = 181.28 (d, $^2J_{C–P}$ = 4.1 Hz), 137.41 (s), 132.19 (s), 129.78 (s), 128.82 (s), 64.12 (d, $^2J_{C–P}$ = 5.3 Hz), 47.16 (s), 16.13 (d, $^3J_{C–P}$ = 7.9 Hz).

II: m.p.: 97 °C. IR (KBr disc, ν, cm^{-1}): 3264, 3094, 2913, 1768, 1550, 1501, 1420, 1332, 1286, 1184, 1107, 1024, 973, 882, 803, 654. MS (70 eV, EI): m/z (%) = 333 (72) $[M + 1]^+$, 332 (75) $[M]^+$, 331 (72) $[M–1]^+$, 122 (72) $[CHNPS_2]^+$, 120 (24) $[NHCH_2C_6H_4CH_3]^+$, 28 (100) $[C_2H_4]^+$. $^{31}P\{^1H\}$ NMR (121 MHz, $CDCl_3$): δ (ppm) = 50.80 (s). ^1H NMR (301 MHz, $CDCl_3$): δ (ppm) = 8.20 (t, J = 2.7 Hz, 1H), 7.76 (d, $^2J_{H–P}$ = 9.7 Hz, 1H), 7.35 (d, $^3J_{H–H}$ = 8.4 Hz, 2H), 7.25 (d, $^3J_{H–H}$ = 8.4 Hz, 2H), 4.82 (apparent d, J = 5.1 Hz, 2H), 4.17 (m, 4H), 2.37 (s, 3H), 1.32 (t, $^3J_{H–H}$ = 7.1 Hz, 6H). $^{13}C\{^1H\}$ NMR (75 MHz, $CDCl_3$): δ (ppm) = 180.84 (d, $^2J_{C–P}$ = 6.3 Hz), 137.62 (s), 133.31 (s), 129.50 (s), 127.71 (s), 64.68 (d, $^2J_{C–P}$ = 5.1 Hz), 50.07 (s), 21.19 (s), 15.80 (d, $^3J_{C–P}$ = 7.9 Hz).

Preparation of $[\{(C_2H_5O)_2P(S)(NC(S)NHCH_2C_6H_4\text{-}4\text{-}Cl)\}_2Ni]$ (III) and $[\{(C_2H_5O)_2P(S)(NC(S)NHCH_2C_6H_4\text{-}4\text{-}CH_3)\}_2Ni]$ (IV). A solution of the ligand (**I** or **II**) in methanol was reacted with a solution of potassium hydroxide in the same solvent (1 : 1 mole ratio). Then, a solution of $NiCl_2 \cdot 6H_2O$ in methanol was added dropwise (ligand : metal mole ratio = 2 : 1), and the solution was stirred for 3 hours. The potassium chloride salt was filtered off, and the filtrate was left until the solvent evaporated. Violet crystals, suitable for X-ray analysis, were obtained from recrystallizing residual precipitate in a mixture of methanol/acetonitrile (1 : 1 v/v).

III: m.p.: 133 °C. IR (KBr disc, ν, cm^{-1}): 3168, 2978, 2914, 1565, 1494, 1394, 1340, 1262, 1093, 1027, 969, 907, 814. $^{31}P\{^1H\}$ NMR (121 MHz, $CDCl_3$): δ (ppm) = 57.32 (s). ^1H NMR (301 MHz, $CDCl_3$): δ (ppm) = 9.42 (s, 2H), 7.25 (d, $^3J_{H–H}$ = 8.1 Hz, 4H), 7.18 (d, $^3J_{H–H}$ = 8.0 Hz, 4H), 4.46 (apparent d, J = 6.0 Hz, 4H), 4.36–3.93 (m, 8H), 1.42 (*t*, $^3J_{H–H}$ = 7.0 Hz, 12H). $^{13}C\{^1H\}$ NMR (75 MHz, $CDCl_3$): δ (ppm) = 187.13 (weak signal), 134.41 (s), 133.78 (s), 128.99 (s), 128.93 (s), 63.17 (d, $^2J_{C–P}$ = 4.7 Hz), 45.21 (s), 15.98 (d, $^3J_{C–P}$ = 8.1 Hz).

IV: m.p.: 134 °C. IR (KBr disc, ν, cm^{-1}): 3180, 2982, 2905, 2861, 1555, 1461, 1404, 1339, 1251, 1162, 1101, 1045, 959, 906, 820, 801, 669. $^{31}P\{^1H\}$ NMR (121 MHz, $CDCl_3$): δ (ppm) = 56.77 (s). ^1H NMR (301 MHz, $CDCl_3$): δ (ppm) = 9.36 (s, 2H), 7.25–7.07 (m, 8H), 4.45 (apparent d, J = 5.8 Hz, 4H), 4.38–3.95 (m, 8H), 2.38 (s, 6H), 1.44 (t, $^3J_{H–H}$ = 7.1 Hz, 12H). $^{13}C\{^1H\}$ NMR (75 MHz, $CDCl_3$): δ (ppm) = 186.79 (weak signal), 137.78 (s), 132.74 (s), 129.51 (s), 127.58 (s), 63.08 (d, $^2J_{C–P}$ = 4.8 Hz), 45.77 (s), 21.18 (s), 16.01 (d, $^3J_{C–P}$ = 8.4 Hz).

Results and discussion

Crystal structure description

Single crystals of ligands **I**/**II**, and complexes **III**/**IV** were obtained from CH_3CN, and CH_3CN/CH_3OH (1 : 1 v/v) solutions, respectively, in the ambient conditions. All four compounds crystallize in the triclinic $P\bar{1}$ space group, with one molecule in the asymmetric units of **I**/**II** and one-half of the molecule in the

asymmetric units of **III**/**IV** (Fig. S1†). The complete molecules of **III** and **IV** are generated by an inversion element.

In these structures, the P atoms have a distorted tetrahedral $P(S)(N)(O)_2$ environment, and the N atom attached to phosphorus is also linked to the carbon atom of a C(S)N moiety. Both these nitrogen atoms in all four structures show almost a planar configuration with the NHC_2, NHPC, or NPCNi environments. The bond lengths and angles are in the normal range of analogous structures and according to the atoms involved.[54,55] In the coordination compounds **III** and **IV**, the nickel atom has a square planar NiS_2N_2 geometry.

After the deprotonation of the P(S)NHC(S) segment (from ligands to complexes), the phosphorus–nitrogen and carbon–nitrogen bonds are strengthened, while the carbon–sulfur bonds are weakened. The related values in **I**/**II** and **III**/**IV** (d_{P-N} = 1.6731 (12)/1.6714 (15) Å & 1.647 (2)/1.646 (2) Å, d_{C-N} = 1.3772 (18)/1.376 (2) Å & 1.343 (4)/1.348 (4) Å, d_{C-S} = 1.6839 (14)/1.6807 (18) Å & 1.727 (3)/1.729 (3) Å) show the changes in carbon–sulfur bonds are higher.

In all structures, the intramolecular N–H···S=P hydrogen bond is made by the NH unit of the X-$C_6H_4CH_2NH$ segment (X = Cl/CH_3), forming a 6-membered hydrogen-bonded ring (an S6 graph-set, graph set notations are described in the ref. 56). Typically, this hydrogen bond in structure **III** is slightly stronger than the associated ligand (**I**) (according to the $V(r)$ = −0.0122/−0.0104 a.u. and $\rho(r)$ = 0.0201/0.0194 a.u. for **III**/**I**). The sulfur atom of the thiocarbonyl group cooperates in the intermolecular N–H···S hydrogen bonds in **I**/**II** or coordination Ni–S bonds in **III**/**IV**. These structural features are also observed in the reported constitutional isomers,[33,34] despite the different packing characteristics due to their different molecular conformations.

The conformations of the P(S)NC(S)N segment are described by the S–P–N–C/P–N–C–N/P–N–C–S torsion angles. These torsion angles show ±sc/+sp/+ap conformations in **I**/**II** and +sp/+sp/+ap conformations in **III**/**IV** (sp = synperiplanar, ap = antiperiplanar, and sc = synclinal). The differences of conformations in ligands and complexes are related to the S=P–N–C torsion angles (**I**/**II**: 48.44°/−50.77°, **III**/**IV**: 13.28°/24.41°), which correspond to an almost flat hydrogen-bonded S6 ring in complexes and higher twisting of the similar ring in ligands. This trend to planarity is a result of the deprotonation of NH units in complexes.

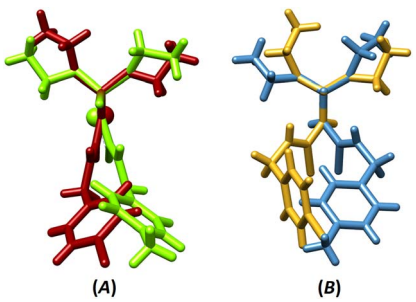

Fig. 1 The overlays of (A) III/IV (RMSD = 0.002) and (B) I/II (RMSD = 0.010) with fixing the PSN moieties on each other (for III/IV, one-half of the molecule was considered).

The superposition of coordination structures (**III** and **IV**, Fig. 1A) shows a relative mirror image relation (if the difference of Cl/CH_3 substituents is ignored). This feature does not appear in the ligand structures (**I** and **II**, Fig. 1B), where the orientations of amine and ethyl groups are different.

The ESP maps of molecules in crystal structures were generated to make a better image of the potential of each part of molecules for establishing interactions (Fig. 2). Accordingly, in the ligand structures, the highest accumulation of negative ESP is around the C=S sulfur atom (the surface energy, E_{sur} = −26.7 and −26.0 kcal mol^{-1} for **I** and **II**). The involvement of the P=S sulfur atom in the intramolecular hydrogen bond decreases the negative ESP accumulation (−14.0 and −14.4 kcal mol^{-1} for **I** and **II**). The positive ESP is accumulated on the P-bonded NH groups (the highest E_{sur} = +29.0 and +27.8 kcal mol^{-1} for **I** and **II**), creating a high potential for establishing intermolecular hydrogen bonds.

In complexes, coordinating the C–S and P-bonded nitrogen atom to the Ni atom reduces the negative ESP of this sulfur atom, and removes the positive ESP around the nitrogen atom. The most negative ESP is located on one of the ethoxy O atoms (the lowest E_{sur} = −23.6 and −28.2 kcal mol^{-1} for **III** and **IV**), while positive ESP is almost uniformly expanded on all CH units. Thus, interactions are weak in the crystals and molecules do not include suitable sites to form prominent interactions.

The ESP surfaces visualize the differences in the Cl/CH_3 behaviors. Negative ESP is distributed as a belt around the Cl atom, and on the σ-hole region, and the absolute value of the negative ESP decreases. This trend is almost reversed for the methyl group. The belt around the CH_3 group contains a positive ESP, while by relocating to the region along the σ-bond, the value of the positive ESP decreases.

A remarkable feature in ESP surfaces is the effect of electronegative atoms on the surrounding environment. In all structures, the ESP on the surface of the side of the aryl ring closer to the sulfur atom is more negative than the other side. In **I** and **II**, the E_{sur} of near/far faces of the aryl ring to the C=S group are equal to −17.3/−10.9, and −22.0/−17.0 kcal mol^{-1}. In **III** and **IV**, unlike **I** and **II**, the P=S group is oriented towards the aryl ring, and the E_{sur} of near/far faces of the aryl ring is equal to −7.7/−4.8, and −13.1/−11.5 kcal mol^{-1}, respectively. In complexes, the cooperation of the electronegative N and S atoms with an oxygen atom situated sterically above them creates a vast region with high negative ESP, which is maximized on the oxygen atom. This region even covers the surroundings of the Ni atom, which individually has a positive charge.

Based on Rozas classification, all of the hydrogen bonds are weak, and positive $\nabla^2\rho(r)$ and $H(r)$ values of all BCPs indicate the absence of any strong/moderate hydrogen bond.[57]

In the molecular assembly of **I**, a dimer synthon ($R_2^2(8)$) is formed through a pair of N–H···S=C hydrogen bonds (the most important interaction, $V(r)$ = −0.0112 a.u., $\rho(r)$ = 0.0224 a.u.), which is strengthened by the C–H···S=C interactions (pair **Ia**, Fig. 3). Such dimers are connected through two equal C–H···O hydrogen bonds ($V(r)$ = −0.0062 a.u., $\rho(r)$ = 0.0089 a.u., pair **Ib**), and construct a tape in the direction of [110]. Weak C–H···N

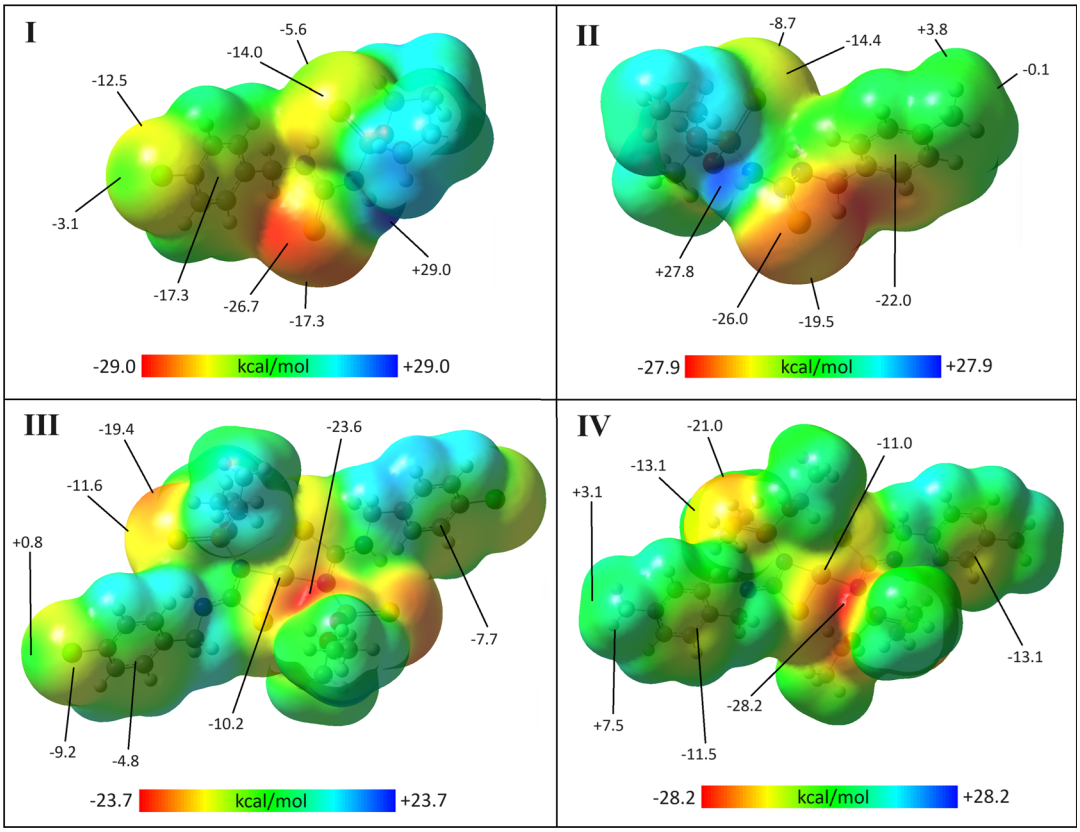

Fig. 2 ESP surfaces of I–IV with the isovalue 0.0004 a.u. The energies (in kcal mol^{-1}) for the selected points of the surfaces are given at the B3LYP/cc-pVDZ level of theory.

hydrogen bond ($V(r) = -0.0037$ a.u., $\rho(r) = 0.0063$ a.u.), C–H···O, and C–H···S=C contacts in pair **Ic**, C–H···π interactions and some weak hydrogen bonds in pair **Id**, and three C–H···S hydrogen bonds in pair **Ie** (Table 2) link the tapes together to make sheets parallel to the *ab*-plane (*ab*-assembly, Fig. 3). The sheets are stacked through π···π interaction, along with the C–H···Cl, and C···Cl in pair **If**, and C–H···S=P, and H···H interactions in pair **Ig**, to form a three-dimensional network (Fig. 3B).

The most important molecular pair in **II** (pair **IIa**, Fig. 4) is similar to **I**, which includes N–H···S=C hydrogen bonds ($V(r) = -0.0109$ a.u., $\rho(r) = 0.0219$ a.u., $R_2^2(8)$ motif), and C–H···S=C interactions. However, the number of the latter type of interactions is different (in comparison with pair **Ia**, Table 2).

Regardless of pair **IIa**, the molecular assembly in **II** is significantly different from **I**. The C–H···O hydrogen bond of pair **IIb** holds the dimers **IIa** together ($V(r) = -0.0073$ a.u., $\rho(r) = 0.0101$ a.u.) to make a one-dimensional assembly along the *a*-axis, which is reinforced by P=S···N, P=S···O, C–H···S=C, and dihydrogen contacts. The C–H···S=P hydrogen bond ($V(r) = -0.0047$ a.u., $\rho(r) = 0.0091$ a.u.) and the interactions related to the aryl fragment (C–H···π, N–H···π, and π···π) in pair **IIc** and the C–H···S=C interactions in pair **IId** extend the supramolecular architecture to a two-dimensional assembly parallel to the *ac*-plane (*ac*-assembly, Fig. 4A). Such symmetry-related sheets are connected through C–H···S=P, C–H···π, and H···H interactions (pairs **IIe** and **IIf**) to form a three-dimensional supramolecular architecture (Fig. 4B).

The molecular packing maps of structures **III** and **IV** have a close similarity (Fig. 5 and 6). In both structures, the most numbers of intermolecular interactions are seen along the *a*-axis, which include C–H···S=P, C–H···O, C–H···Ni, C–H···N, and C–H···π interactions (pairs **IIIa** and **IVa**, Fig. 5). The planar environments at N and Ni atoms and the high electrostatic potential of the $[(CNHC(S)NP(S))_2Ni]$ part (Fig. 2) influence the formation of ribbon arrangements shown as green and purple in Fig. 5A. In these pairs, the strongest interactions (based on potential energy density) are the C–H···S=P (**IIIa**) and C–H···O (**IVa**) hydrogen bonds with the $V(r)$ values of −0.0035 and −0.0045 a.u., respectively. The intermolecular anagostic C–H···Ni interactions are seen in **III**/**IV** ($V(r) = -0.0032/-0.0027$ a.u. and $\rho(r) = 0.0062/0.0057$ a.u.). The lengths and angles of the C–H···Ni interactions in **III**/**IV** stand 2.946/3.010 Å and 122.31°/113.05°, respectively, which are in the normal range of such rarely occurred interactions (2.3–3.0 Å and 110–170°).[58,59] The ESP surfaces show that the formation of C–H···Ni interactions is related to the electrostatic nature caused by the electronegative atoms neighbor to Ni, which make a vast region with negative electrostatic potential and attracts hydrogens.

The noted assemblies are extended to two-dimensional architectures by the C–H···S=P hydrogen bonds in the directions parallel to the *ac* plane for **III** and $(0\bar{1}1)$ plane for **IV** [Fig. 5,

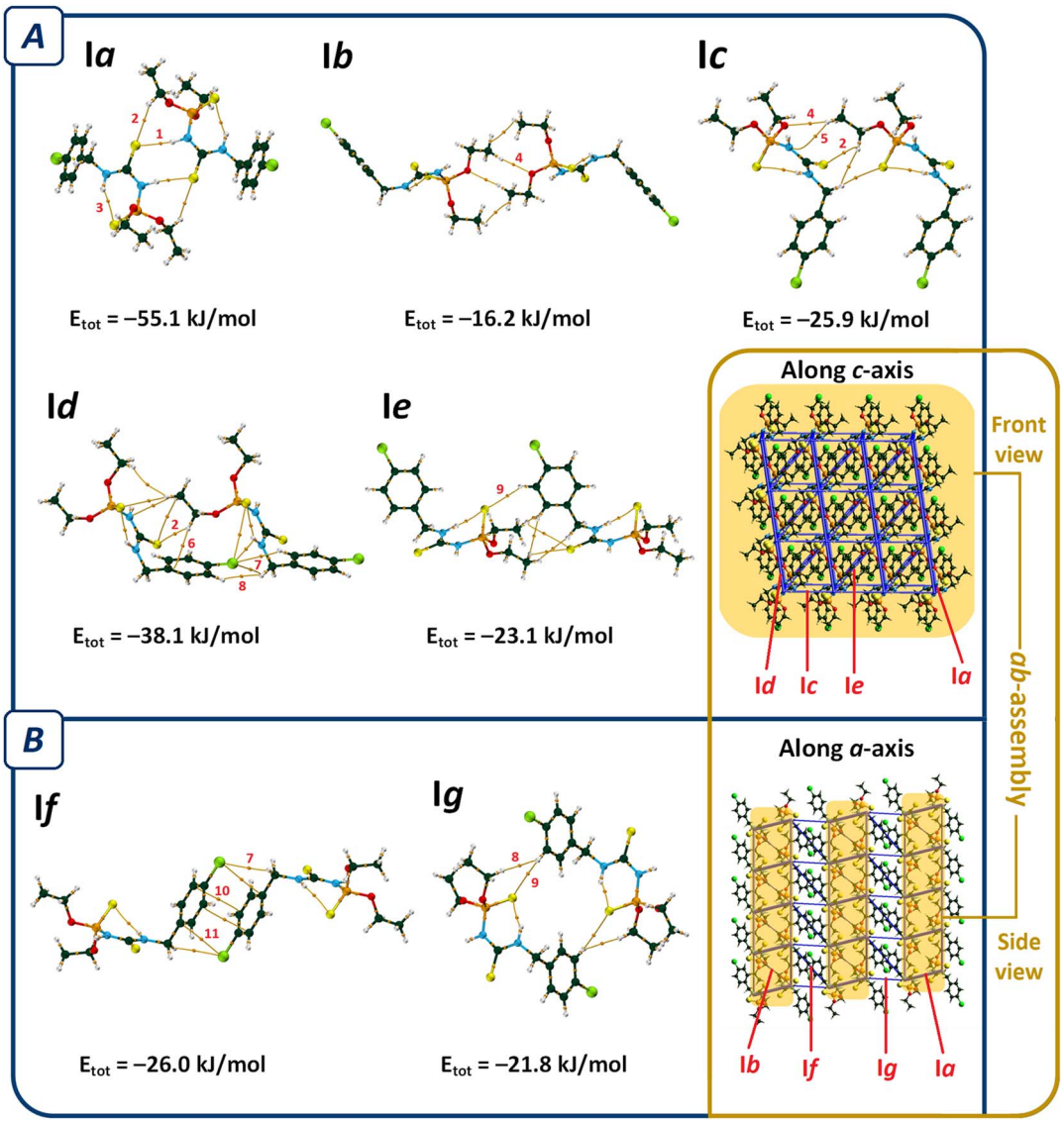

Fig. 3 QTAIM diagrams of the most influential molecular pairs (cutoff energy value = −15 kJ mol^{-1}) in the packing of structure **I**, and two views of the energy framework considering these molecular pairs along the *c*- and *a*-axes. The most prominent interactions in each pair are labeled: NH···S=C (1), CH···S=C (2), NH···S=P (3), CH···O (4), CH···N (5), CH···π (6), CH···Cl (7), H···H (8), CH···S=P (9), π···π (10), and Cl···C (11). Total interaction energies (E_{tot}) are given at the bottom of each pair. Section (A) shows pairs contributing to form *ab*-assembly and section (B) represents pairs that stack *ab*-assemblies together (atom color codes: P = orange, O = red, N = cyan, C = dark green, Cl = light green, S = yellow, and H = white).

$V(r)$ = −0.0041, −0.0017 (pair **IIIb**), −0.0018 and −0.0017 a.u. (pair **IVb**)]. The thiophosphoryl group contributes to some other C–H···S=P interactions, as represented in pairs **IIIc**, **IIId**, and **IVd** (Fig. 6). The stabilization of **III** in the *b*-direction and **IV** in the *c*-direction is happened by C–H···O and CH···HC interactions between two ethoxy groups (pairs **IIIe** and **IVe**, $V(r)$ values are given in Table 2) to form three-dimensional networks altogether with the other noted interactions.

The main difference in the structures originates from the interactions related to the 4-chlorobenzyl and 4-methylbenzyl moieties (**IIIf** and **IVf**). The $CH_2C_6H_4Cl$ and $CH_2C_6H_4CH_3$ moieties in **III** and **IV** take part in similar contacts to the associated ligands, *i.e.* C–H···Cl/π···π and two equal C–H···π interactions, respectively (Fig. 6).

In pair **IVf**, there is a slippage between two adjacent arene rings compared to **IIIf**. This slippage also changes the orientation of the ethoxy groups. The conformation of the P–O–C–C segments are +ap/+ap for **III** and +ap/+ac (ac = anticlinal) for **IV**. The different conformations cause a larger distance of chlorine and ethoxy with respect to the methyl and ethoxy groups in associated compounds. However, the chlorine atom attracts one of the terminal hydrogen atoms of the ethoxy group and makes a C–H···Cl hydrogen bond (Fig. 6, $V(r)$ = −0.0026 a.u., $\rho(r)$ = 0.0050 a.u.). In the lack of the chlorine atom (in **IV**), the CH_2

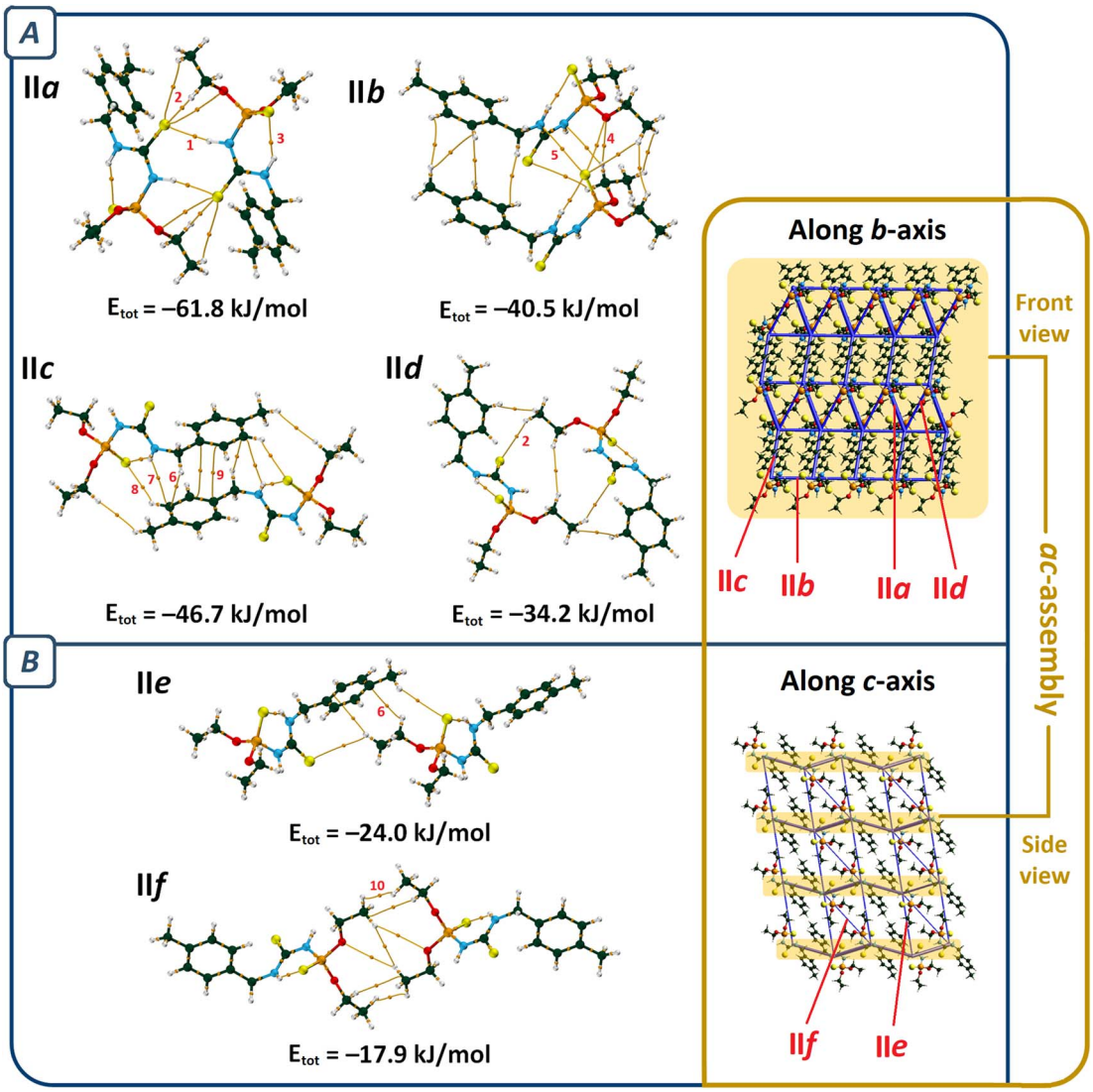

Fig. 4 QTAIM diagrams of the most influential molecular pairs (cutoff energy value = −15 kJ mol^{-1}) in the packing of structure II, and two views of the energy framework considering these molecular pairs along the *b*- and *c*-axes. Total interaction energies (E_{tot}) are given at the bottom of each pair. The most prominent interactions in each pair are labeled: NH···S=C (1), CH···S=C (2), NH···S=P (3), CH···O (4), S···N (5), CH···π (6), NH···π (7), CH···S=P (8), π···π (9), and H···H (10). Section (A) shows pairs contributing to form *ac*-assembly, and section (B) represents pairs that stack *ac*-assemblies together (atom color codes: P = orange, O = red, N = cyan, C = dark green, S = yellow, and H = white).

unit of benzyl takes part in the C–H···π interaction; thus, the closeness of the ethoxy and methyl groups forces the ethoxy group backward.

Considerable differences in the crystal packings of **I** and **II** are reflected in the pronounced differences in the volumes of unit cells (801.93 (3) and 822.58 (4) Å^3). While **III** and **IV** (with more similarities) show comparable volumes (835.66 (5) and 835.21 (6) Å^3).

Analysis of contacts using fingerprint plots

The 2D fingerprint plots illustrate the contribution rates of contacts in molecular packing, as shown in Fig. 7. In all structures, H···H contacts have more share relative to the other contacts and are developed in a vast region of plots. These contacts relative to total contacts have 41.8% in **I** and 46.5% in **III**, with the Cl substituent, and increase to 60.9% in **II** and 61.2% in **IV**, with the CH_3 group. The smallest corresponding d_i + d_e values are marked with label 1 in the figure.

The sum of H···H% and Cl···H% contacts in **I** and **III** are comparable with the percentages of H···H contacts in **II** and **IV**. This value for the structure **I** (H···H% + Cl···H% = 55.6%) is remarkably lower than H···H% in the structure **II** (H···H% = 60.9%). Part of this difference is due to the π···π interactions, which are fewer in **II** with respect to **I** (C···C% = 0.3% and 2.6%). The environment around the chlorine atom in **III** does not have any notable difference relative to the methyl group in **IV** (**III:** H···H% + Cl···H% = 61.1%, **IV:** H···H% = 61.2%), which is a result of the almost similar molecular packing.

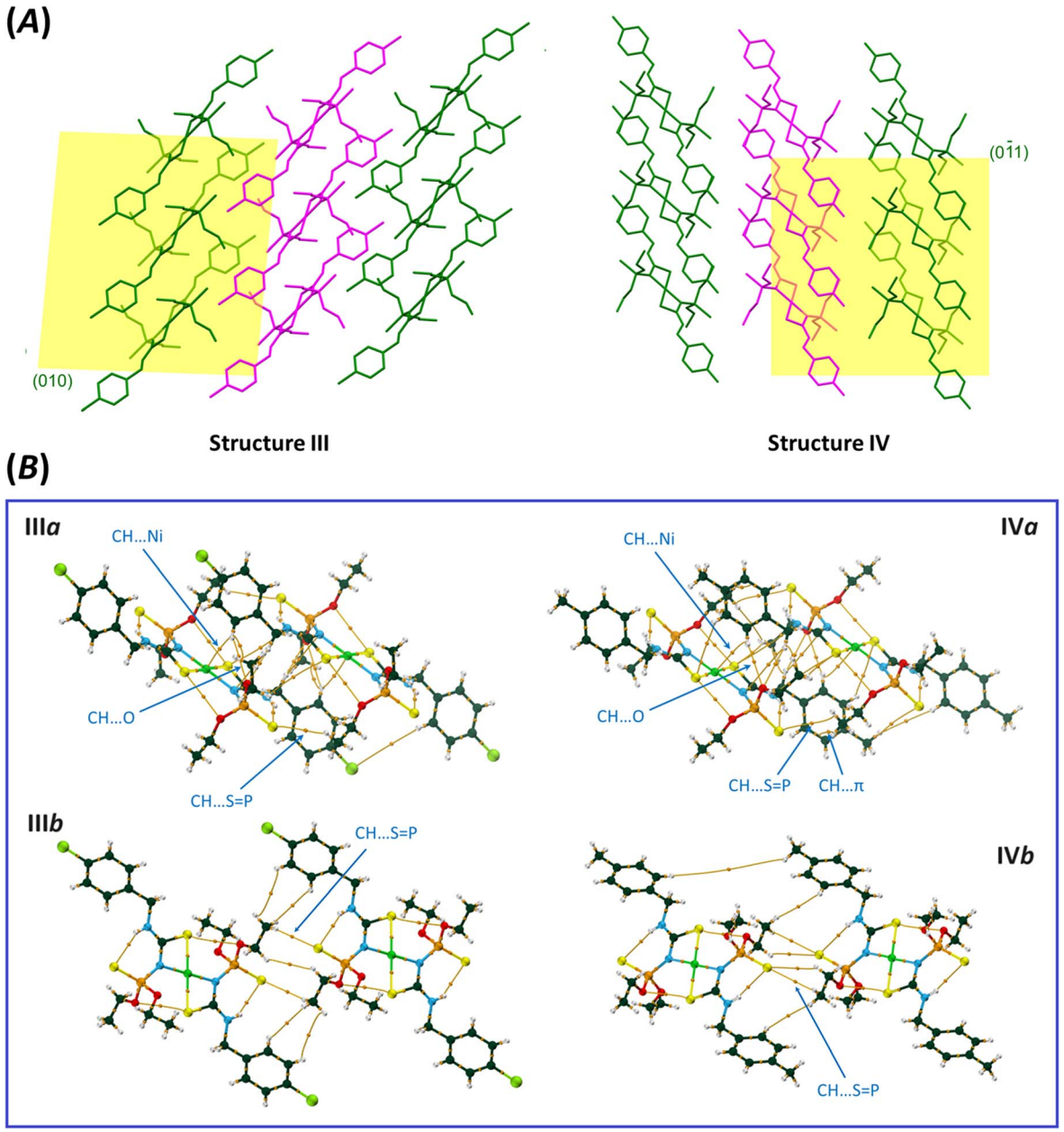

Fig. 5 (A) Two-dimensional assemblies formed by the molecular pairs **IIIa**/**IIIb** and **IVa**/**IVb**. Ribbons, represented by green and purple colors, constructed through the consequence of pairs **IIIa** and **IVa**; molecules in the ribbons with different colors interacted together as shown in the pairs **IIIb** and **IVb**. (B) QTAIM diagrams of the molecular pairs **IIIa**/**IVa** and **IIIb**/**IVb** (atom color codes: Ni = green, P = orange, O = red, N = cyan, C = dark green, S = yellow, Cl = light green, and H = white).

The contribution of the arene rings in the molecular packing (π···π/C–H···π) appears as C···C and C···H contacts (labels 3 and 4). In two structures having chlorine atoms (**I** and **III**), the arene rings take part in π···π interaction, while in the analogous structures having methyl groups (**II** and **IV**), the π···π interactions do not matter (C···C is absent in **IV**). This scarcity/absence of π···π interactions in **II**/**IV** is compensated by raising the C–H···π interactions.

In **I**/**II**, the H···S contacts appear as the tallest spikes (with $d_i + d_e \approx 2.3$–2.5, label 5) due to the N–H···S=C hydrogen bonds, while in **III**/**IV**, the weak C–H···S=P hydrogen bonds appear as shorter spikes (with $d_i + d_e \approx 2.8$–3.0). The H···O contacts manifest two small symmetric spikes in all structures (label 6). The C–H···N contacts in **III**, and C–H···Ni contacts in **III**/**IV** have small contributions, which are introduced with labels 7 and 8, respectively (Fig. 7).

Study of the origin of similarities/differences in packing features

Scrutinizing intermolecular interactions in analogous structures helps to understand the origin of changes in the packing features. Structures **III** and **IV** have very slight variances, while **I**

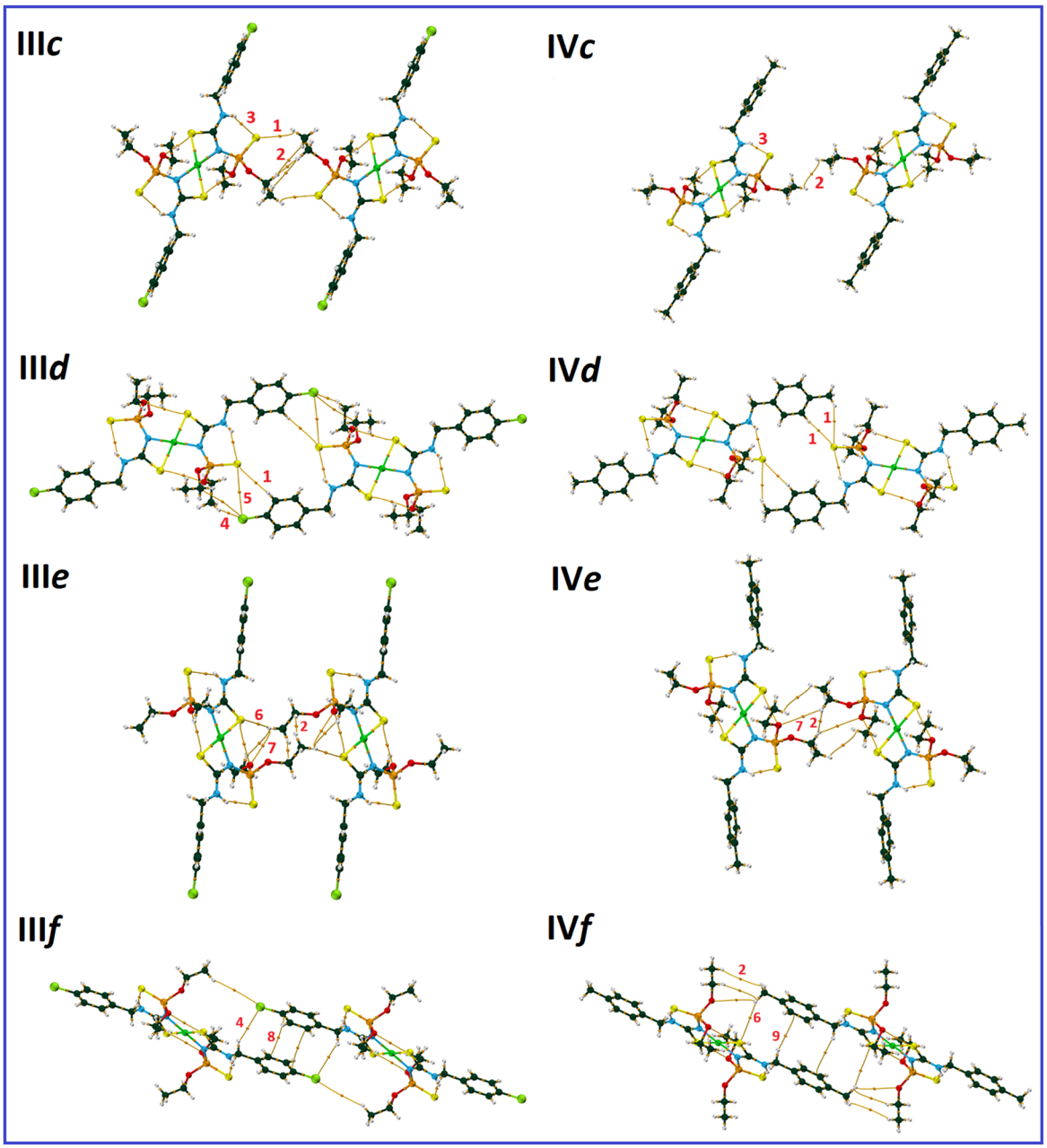

Fig. 6 QTAIM diagrams of the molecular pairs **IIIc–IIIf** and **IVc–IVf** (atom color codes: Ni = green, P = orange, O = red, N = cyan, C = dark green, S = yellow, Cl = light green, and H = white). The most prominent interactions in each pair are labeled: CH···S=P (1), H···H (2), NH···S=P (3), CH···Cl (4), S···Cl (5), CH···S–C (6), CH···O (7), π···π (8), and CH···π (9).

and **II** differ significantly. On the other hand, the supramolecular networks of **III** and **IV** are negligibly affected by the Cl/CH_3 substituents. Notably, in pairs **IIIa** and **IVa**, with the most contact surfaces (covering 43.2% and 35.9% of the Hirshfeld surfaces of **III** and **IV**, respectively) and the majority of interactions, the Cl/CH_3 substituents do not have a significant role in the formation of the assemblies. Structures **I** and **II** have completely different packing features. Hence, it stands to reason that the change of substituent (Cl/CH_3) will determine the difference between the crystal packing features.

A common characteristic of the structures reported here (**I–IV**) is the intramolecular N–H···S=P hydrogen bonds, similar to most of the analogous structures retrieved from the Cambridge Structural Database.[60] In structures **I** and **II**, the centrosymmetric hydrogen-bonded dimers are formed through a pair of N–H···S=C hydrogen bonds. Other packing features are different and heavily depend on the Cl/CH_3 substituents.

The results of crystal lattice energy calculations demonstrate that structure **I** has a much bigger amount of attraction force (E_{att}) than structure **II** ($E_{att} = \frac{1}{2}\sum NE^*_{att}$, in which $E^*_{att} = E_{ele} + E_{pol} + E_{dis}$, $E_{att(I)} = -301.2$ kJ mol^{-1}, $E_{att(II)} = -279.4$ kJ mol^{-1}), counteracting with repulsion force, despite the crystal lattice energy of **II** is slightly larger ($E_{latt(I)} =$

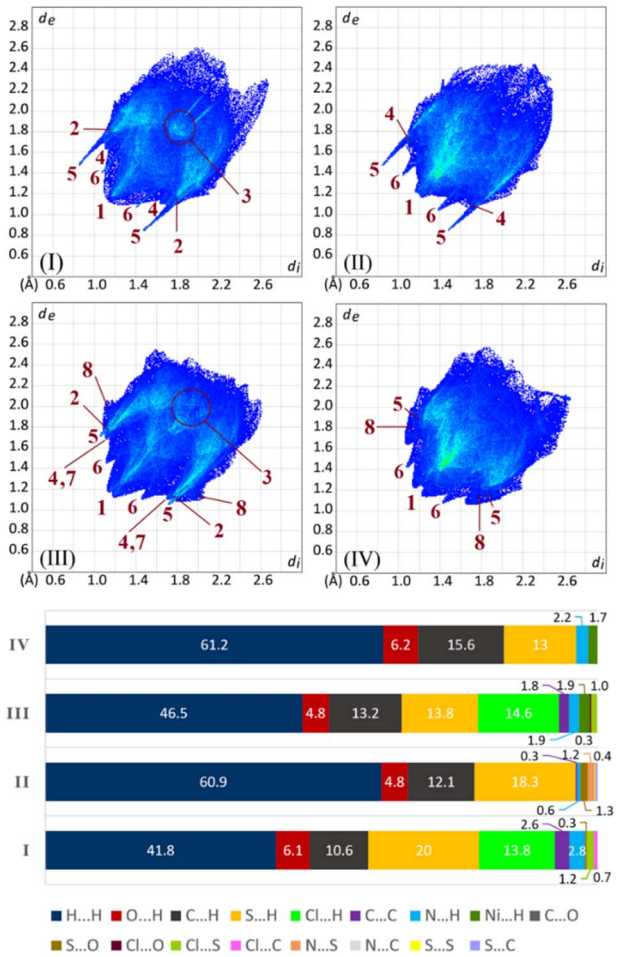

Fig. 7 2D fingerprint plots and percentages of contacts in structures I–IV. Locations of corresponding minima $d_i + d_e$ values for contacts are shown by the numbers (contact codes: 1 = H···H, 2 = Cl···H, 3 = C···C, 4 = C···H, 5 = S···H, 6 = O···H, 7 = N···H, and 8 = Ni···H).

-164.8 kJ mol^{-1}, and $E_{\text{latt(II)}} = -166.8$ kJ mol^{-1}). The greater attraction force of **I** (arising from interactions of Cl substituent) results in denser molecular packing (the volumes within Hirshfeld surfaces for **I** and **II** equal 392.83 and 403.22 Å^3, respectively). In such conditions, investigating the interactions of the altered fragments (aryl groups) in these two structures can shed light on factors affecting changes in molecular packing features.

In structure **I**, the most important interactions around the aryl fragment include π···π with two near C···C bond paths ($V(r)$ = -0.0022 a.u.), a pair of equal C–H···Cl interactions ($V(r)$ = -0.0034 a.u., pair **If**, Fig. 3), and a C–H···π interaction (pair **Id**, $V(r)$ = -0.0033 a.u., Fig. 3). Moreover, the chlorine atom is involved in hydrogen bonding with three near hydrogen atoms (pair **Id**, Fig. 3).

In structure **II**, the environment around the aryl fragment exhibits some variations. Despite the presence of the C–H···π contacts formed by two hydrogens of the ethyl fragment (pair **IIe**, $V(r) = -0.0025$ and -0.0020 a.u., Fig. 4), the behavior of the aryl fragment in interacting with one another differs from the structure **I**. In this structure, the aryl rings interact by a pair of equal C–H···π interactions (pair **IIc**, Fig. 4), along with a π···π interaction with fewer potential energy density ($V(r) = -0.0019$ a.u. for two observed bond paths).

Thus, the chlorine atom in **I** with higher electrostatic potential has the propensity to establish weak hydrogen bonds (C–H···Cl with $V(r) = -0.0034$, -0.0025, and -0.0022 a.u. and N–H···Cl with $V(r) = -0.0021$ a.u., pairs **Id** and **If**). Especially in pair **If**, it creates a motif that is stabilized by the cooperation of a π···π interaction; while in **II**, the CH_3-substituent with lower electrostatic potential is not involved in such interactions. The interactions of the CH_3 substituent are weaker and in lack of Cl-involved hydrogen bonds, the molecules have more freedom to form different competing interactions. Especially in pair **IIc**, aryl fragments are stacked through C–H···π and π···π interactions. Hence, the electrostatic differences of the CH_3/Cl substituents lead to the different packing features of **I** and **II**.

Structures **III** and **IV** have nearly identical molecular packing; however, similar to structures **I** and **II**, the mutual interactions of aryl fragments are different. These fragments in structures **III** and **IV** make contacts almost resembling **I** and **II**, respectively. In structure **III**, dimers are formed through π···π and C–H···Cl interactions (pair **IIIf**), while in structure **IV**, analogous dimers (pair **IVf**) are constructed through C–H···π and H_2C–H···S–C interactions, and the π···π interactions are absent.

Similar supramolecular motifs related to the $CH_2C_6H_4Cl$ fragment (involving C–H···Cl and π···π interactions) were also observed in the structures with the refcodes HELXAB and HELXEF (with the formulas $P(S)(NHCH_2C_6H_4Cl)_3$ and $[P(S)(NHCH_2C_6H_4Cl)_3]_2Hg_2Cl_4$, respectively).[40]

As a result, the role of the electrostatic potential is crucial in these variations. Hydrogens in all structures tend to interact with groups having high negative ESP values. In the aryl fragment of structures **I** and **III**, the Cl atom has a high negative ESP, but in the absence of the Cl atom in **II** and **IV**, the π-electron cloud is more negative, which attracts the hydrogen atoms.

To make a more comprehensive evaluation of the repeatability of these patterns, a survey in the CSD was conducted based on the structures having $CH_2C_6H_4$-4-Cl and $CH_2C_6H_4$-4-CH_3 fragments. The first search was carried out based on the motifs containing two $CH_2C_6H_4$-4-Cl moieties interacted with two C···C contacts (between two carbons in positions of 2 or 3 of aryl rings) within the specified distance ≤ 3.8 Å. The second search was done based on the motifs including two $CH_2C_6H_4$-4-CH_3 moieties, which have at least two reciprocal C···H contacts (between a carbon atom in any position of aryl ring and a hydrogen of CH_2 unit) with a distance ≤ 3.3 Å.

Among structures that possess $CH_2C_6H_4$-4-Cl fragment, 142 queries out of 844 have patterns similar to those in the structures **I** and **III** (containing π···π interactions with C···C distances up to 3.8 Å and C–H···Cl hydrogen bond, Fig. 8), which shows 17% probability of repetition of these motifs. Fig. 8 shows the frequency of π···π interaction lengths of the specified patterns. Accordingly, the lengths of π···π

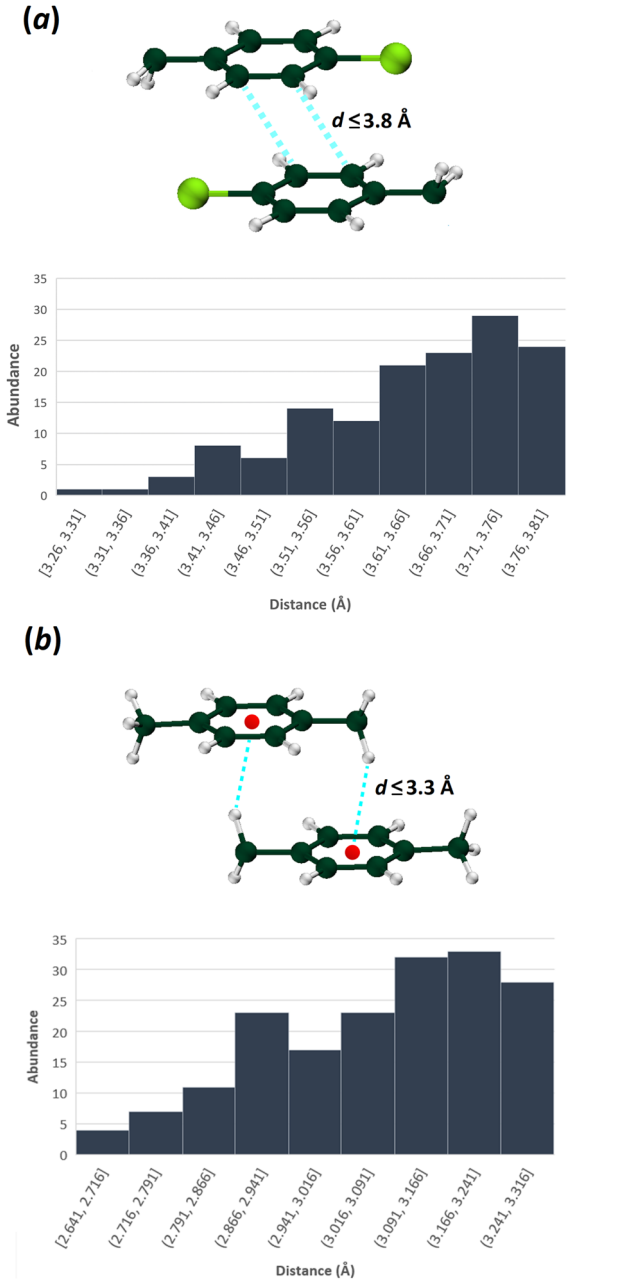

Fig. 8 The distribution of indicated interaction lengths between (a) two $CH_2C_6H_4Cl$, and (b) two $CH_2C_6H_4CH_3$ fragments (CSD version 5.42 updated at September 2021 was used).

interactions in structures **I** and **III** are within the normal range (Cg···Cg = 3.640 and 3.644 Å, respectively).

For the structures with the $CH_2C_6H_4$-4-CH_3 fragment, 178 queries out of 1482 have patterns similar to those in structures **II** and **IV** (*i.e.*, a 12% probability of repeating, applying a criterion of C···H distances up to 3.3 Å). As was noted earlier, this motif includes a pair of equal C–H···π interactions, with the CH_2 moiety as a hydrogen bond donor (Fig. 8). According to the abundance histogram, the C–H···π interaction length in the structures **II** and **IV** is in the normal range (C–H···C = 2.841 and 3.198 Å).

Spectroscopy

In the IR spectra, the bands centered at 3258/3099 cm^{-1} for **I** and 3264/3094 cm^{-1} for **II** are associated with the NH vibrations. For the related nickel complexes, only one band appears in this region, centered at 3168 cm^{-1} for **III** and 3180 cm^{-1} for **IV** (due to the deprotonation of one NH unit in the coordinated ligand). For **I** and **II**, the bands at 1552 and 1550 cm^{-1} are related to the S=C–N vibration that for **III** and **IV** are shifted to 1565 and 1555 cm^{-1}, similar to those reported for analogous ligands/complexes.[32]

The phosphorus signals appear as a singlet (in $^{31}P\{^1H\}$ NMR) at 60.57 and 50.80 ppm for **I** and **II** and 57.32 and 56.77 ppm for **III** and **IV**, respectively (solvent: DMSO-d_6 for **I** and $CDCl_3$ for **II**, **III**, and **IV**).

In the ^1H NMR spectra, triplets in the range of 1.27–1.44 ppm and multiplets in the range of 3.93–4.38 ppm correspond to the CH_3 and CH_2 moieties of ethyl groups. The CH_2 moiety of the benzyl group appears as a doublet (within 4.45–4.82 ppm). A typical pattern of the *para*-substituted arene ring (two doublets) is observed for **I–III** in the 7.18–7.43 ppm range, but in **IV**, an overlap signal appears at 7.25–7.07 ppm.

The shapes of NH signals are surprising, as they show the effects of hydrogen bonding, complexation, and solvent. For **I** (in DMSO-d_6), the triplet at 8.55 ppm corresponds to the NH unit that bonded to the CH_2 moiety, and the broad peak at 9.33 ppm corresponds to the NH unit of the P(S)NHC(S) segment. For **II** (in $CDCl_3$), the NH unit bonded to the CH_2 moiety appears a triplet, slightly shifted with regard to **I** (at 8.20 ppm); however, the shift and pattern of the other NH unit are meaningful (at 7.76 ppm as a doublet with J = 9.7 Hz). These differences are related to the solvent effect and different hydrogen bonding in the two solvents. The pattern of the noted triplet in $CDCl_3$ is also different from the triplet in DMSO-d_6, where in $CDCl_3$, it tends to broaden, probably due to the remaining intramolecular NH···S hydrogen bonding, and the through space phosphorus nucleus effect to this NH unit. In both complexes, only one broad NH signal appears at 9.42 ppm for **III** and 9.36 ppm for **IV** (complexes lack the other NH). The broadening is related to the remaining NH···S hydrogen bonds in solution, which are stronger in complexes with respect to the corresponding ligands.

In the $^{13}C\{^1H\}$ NMR spectra of all four compounds, the CH_3 and CH_2 groups (of ethyl moiety) and the CS group appear as doublets, due to ^3J coupling with phosphorus for methyl and ^2J couplings for two others. Typically, for **I**, the related signals appear at 16.13 ($^3J_{CP}$ = 7.9 Hz), 64.12 ($^2J_{CP}$ = 5.3 Hz), and 181.28 ppm ($^2J_{CP}$ = 4.1 Hz). The chemical shifts and coupling constants related to similar carbon atoms in three other compounds show no significant differences, except for low-intensity signals of CS units in complexes. The other aliphatic/aromatic signals appear as singlets at the expected regions, as noted in the Experimental section.

Conclusions

The $(C_2H_5O)_2P(S)(NHC(S)NHCH_2C_6H_4X)$ thiophosphoramides and the $[\{(C_2H_5O)_2P(S)(NC(S)NHCH_2C_6H_4X)\}_2Ni]$ complexes (X

= Cl/CH_3, **I**/**II** and **III**/**IV**) were synthesized to study the effect of the Cl/CH_3 substituents in the crystal packing. Despite the same crystallization process, the molecular packing features are different in the ligands but are similar in the complexes. These characteristics can be monitored by comparing the degrees of participation of the Cl···H and H···H contacts with the H···H contacts, respectively in compounds including the chlorine substituents (**I**/**III**) with analogous CH_3-substituted compounds (**II**/**IV**) by the Hirshfeld surface analyses. The sum of Cl···H% and H···H% percentages in **I** is different from the H···H% in **II**, but nearly equal sum values are observed in **III** and **IV**. The other feature is different unit cell volumes of the ligands and similar ones of the complexes.

By analyzing crystal structures, the origins of the similarities/differences were investigated, and the following conclusions were drawn: in the ligands, the dimer synthons are formed through classical N–H···S=C hydrogen bonds, and to connect the dimers some weak interactions compete with each other. Thus, the variations in the molecular packing features are brought about by the Cl and CH_3 substituents, which have different capacities for establishing interactions. In structure **I**, the chlorine atom takes part in the C–H···Cl hydrogen bonds, which drives the aryl rings to stack through π···π interactions. In structure **II** with the CH_3 substituent, the molecules take part in C–H···π and π···π interactions.

In the molecular complexes, the planar environment around N and Ni atoms, the electron delocalization in the NCS segment, and intramolecular N–H···S=P hydrogen bonds cause the planarity and rigidity of the middle part of the molecule (*i.e.* the [(CNHC(S)NP(S))$_2$Ni] fragment). These geometry requirements and high negative electrostatic potential in this region cause to attract hydrogens and make CH···O, CH···N, CH···Ni, and CH···S interactions, which facilitate molecular stacking and the creation of ribbon assemblies. A large part of the interactions is established in these ribbons without the contribution of the Cl/CH_3 substituents. Consequently, despite the lack of moderate interactions in **III** and **IV**, several numbers of weak interactions contribute to constructing the main feature of supramolecular assembly. Thus, the structures become strikingly alike. The slight differences in the structures arise from the slippage of the $CH_2C_6H_4CH_3$ moieties in **IV** relative to the $CH_2C_6H_4Cl$ moieties in **III**, which causes the different conformations of ethoxy groups.

Altogether, it can be concluded that as much as the role of stronger directional interactions (than those established by Cl/CH_3 groups) in the expansion of the structure in different dimensions decreases, the influence of the Cl/CH_3 exchange on the structural change increases. From the viewpoint of motifs made by aryl groups, the structures **III** and **IV** are similar to the corresponding ligands **I** and **II**.

The variations observed in the aryl···aryl motifs in structures possessing Cl substituent (**I** and **III**) in comparison to structures with CH_3 substituent (**II** and **IV**) may be attributed to the higher negative ESP of the Cl atom relative to the CH_3 group. In the presence of the Cl atom, the hydrogens are preferentially attracted to the Cl, as a part of the negative charge of the π-system is transferred to the Cl atom. Thus, the motifs are constructed through CH···Cl and π···π interactions. In the absence of Cl, the hydrogens are attracted to the π-cloud of the aryl ring to form CH···π interactions.

The analysis of structures possessing $CH_2C_6H_4Cl$ and CH_2-$C_6H_4CH_3$ moieties retrieved from the CSD show around 17% and 12% repeatability of aryl···aryl motifs similar to those observed in **I**/**III** and **II**/**IV**, respectively.

Data availability

The data supporting this article have been included as part of the ESI.† Crystallographic data for **I–IV** have been deposited at the CCDC under CCDC numbers 2311920–2311923.†

Author contributions

Saeed Hosseinpoor (investigation, formal analysis, software, writing – original draft), Mehrdad Pourayoubi (project administration, writing – review & editing), Eliška Zmeškalová (formal analysis (X-ray crystallography), review & editing), Morgane Poupon (formal analysis (X-ray crystallography)).

Conflicts of interest

There are no conflicts to declare.

Acknowledgements

Financial support for this work by the Ferdowsi University of Mashhad is gratefully acknowledged (Project No. 56293/3). This research was supported by the project TERAFIT – CZ.02.01.01/00/22_008/0004594 and by the Czech Science Foundation project 24-10558S.

References

1 Q. Zhu and S. Hattori, *J. Mater. Res.*, 2023, **38**, 19–36.
2 S. M. Woodley and R. Catlow, *Nat. Mater.*, 2008, **7**, 937–946.
3 M. K. Corpinot and D.-K. Bučar, *Cryst. Growth Des.*, 2019, **19**, 1426–1453.
4 M. A. Neumann, J. van de Streek, F. P. A. Fabbiani, P. Hidber and O. Grassmann, *Nat. Commun.*, 2015, **6**, 7793.
5 C. B. Aakeröy, S. Panikkattu, P. D. Chopade and J. Desper, *CrystEngComm*, 2013, **15**, 3125–3136.
6 M. Pourayoubi, M. Toghraee, J. Zhu, M. Dušek, P. J. Bereciartua and V. Eigner, *CrystEngComm*, 2014, **16**, 10870–10887.
7 T. Steiner, *Angew. Chem., Int. Ed.*, 2002, **41**, 48–76.
8 G. R. Desiraju, *J. Am. Chem. Soc.*, 2013, **135**, 9952–9967.
9 Y. Lu, J. Lin, L. Wang, L. Zhang and C. Cai, *Chem. Rev.*, 2020, **120**, 4111–4140.
10 W.-L. Guan, J.-F. Chen, J. Liu, B. Shi, H. Yao, Y.-M. Zhang, T.-B. Wei and Q. Lin, *Coord. Chem. Rev.*, 2024, **507**, 215717.
11 I. Bouabdallah, T. Harit, M. Rahal, F. Malek, M. Tillard and D. Eddike, *Acta Chim. Slov.*, 2021, **68**, 718–727.
12 C.-H. Kuo, D.-C. Huang, W.-T. Peng, K. Goto, I. Chao and Y.-T. Tao, *J. Mater. Chem. C*, 2014, **2**, 3928–3935.

13 G. Cavallo, P. Metrangolo, R. Milani, T. Pilati, A. Priimagi, G. Resnati and G. Terraneo, *Chem. Rev.*, 2016, **116**, 2478–2601.
14 O. Loveday and J. Echeverría, *Nat. Commun.*, 2021, **12**, 5030.
15 H.-Y. Zhuo, L.-X. Jiang, Q.-Z. Li, W.-Z. Li and J.-B. Cheng, *Chem. Phys. Lett.*, 2014, **608**, 90–94.
16 S. E. Wheeler and K. N. Houk, *J. Chem. Theory Comput.*, 2009, **5**, 2301–2312.
17 S. E. Wheeler, *Acc. Chem. Res.*, 2013, **46**, 1029–1038.
18 S. E. Wheeler, *J. Am. Chem. Soc.*, 2011, **133**, 10262–10274.
19 A. Kitaigorodsky, *Molecular Crystals and Molecules*, Academic Press, New York, 1st edn, 1973.
20 A. Nangia, *New J. Chem.*, 2000, **24**, 1049–1055.
21 G. R. Desiraju and J. A. R. P. Sarma, *J. Chem. Sci.*, 1986, **96**, 599–605.
22 M. R. Edwards, W. Jones, W. D. S. Motherwell and G. P. Shields, *Mol. Cryst. Liq. Cryst. Sci. Technol., Sect. A*, 2001, **356**, 337–353.
23 S. Hosseinpoor, M. Pourayoubi, M. Abrishami, M. Sobati, F. Karimi Ahmadabad, F. Sabbaghi, M. Nečas, M. Dušek, M. Kučeráková and M. Kaur, *CrystEngComm*, 2023, **25**, 2557–2569.
24 A. Singh, A. Ramanan and D. Bandyopadhyay, *Cryst. Growth Des.*, 2011, **11**, 2743–2754.
25 A. K. S. Romasanta, D. Braga, M. T. Duarte and F. Grepioni, *CrystEngComm*, 2017, **19**, 653–660.
26 S. Ranjan, R. Devarapalli, S. Kundu, S. Saha, S. Deolka, V. R. Vangala and C. M. Reddy, *IUCrJ*, 2020, **7**, 173–183.
27 S. L. Tan and E. R. T. Tiekink, *CrystEngComm*, 2021, **23**, 1723–1743.
28 M. R. Edwards, W. Jones and W. D. S. Motherwell, *CrystEngComm*, 2006, **8**, 545–551.
29 N. K. Nath and A. Nangia, *Cryst. Growth Des.*, 2012, **12**, 5411–5425.
30 M. Polito, E. D'Oria, L. Maini, P. G. Karamertzanis, F. Grepioni, D. Braga and S. L. Price, *CrystEngComm*, 2008, **10**, 1848–1854.
31 D. A. Safin, M. G. Babashkina, M. Bolte and Y. Garcia, *CrystEngComm*, 2012, **14**, 774–778.
32 D. A. Safin, M. G. Babashkina, M. P. Mitoraj, P. Kubisiak, K. Robeyns, M. Bolte and Y. Garcia, *Inorg. Chem. Front.*, 2016, **3**, 1419–1431.
33 K. E. Metlushka, D. N. Sadkova, L. N. Shaimardanova, K. A. Nikitina, K. A. Ivshin, D. R. Islamov, O. N. Kataeva, A. V. Alfonsov, V. E. Kataev, A. D. Voloshina, L. N. Punegova and V. A. Alfonsov, *Inorg. Chem. Commun.*, 2016, **66**, 11–14.
34 O. N. Kataeva, K. E. Metlushka, Z. R. Yamaleeva, K. A. Ivshin, A. G. Kiiamov, O. A. Lodochnikova, K. A. Nikitina, D. N. Sadkova, L. N. Punegova, A. D. Voloshina, A. P. Lyubina, A. S. Sapunova, O. G. Sinyashin and V. A. Alfonsov, *Cryst. Growth Des.*, 2019, **19**, 4044–4056.
35 R. C. Luckay, X. Sheng, C. E. Strasser, H. G. Raubenheimer, D. A. Safin, M. G. Babashkina and A. Klein, *Dalton Trans.*, 2009, 4646–4652.
36 I. D. Rojas-Montoya, A. Santana-Silva, V. García-Montalvo, M.-Á. Muñoz-Hernández and M. Rivera, *New J. Chem.*, 2014, **38**, 4702–4710.
37 V. Flores-Romero, O. L. García-Guzmán, A. Aguirre-Bautista, I. D. Rojas-Montoya, V. García-Montalvo, M. Rivera, O. Jiménez-Sandoval, M.-Á. Muñoz-Hernández and S. Hernández-Ortega, *New J. Chem.*, 2020, **44**, 10367–10379.
38 M. P. Mitoraj, M. G. Babashkina, A. Y. Isaev, Y. M. Chichigina, K. Robeyns, Y. Garcia and D. A. Safin, *Cryst. Growth Des.*, 2018, **18**, 5385–5397.
39 M. P. Mitoraj, F. Sagan, M. G. Babashkina, A. Y. Isaev, Y. M. Chichigina and D. A. Safin, *Eur. J. Org. Chem.*, 2019, **2019**, 493–503.
40 M. Khorramaki, M. Abad, V. Darugar, M. Pourayoubi, M. Vakili, M. Nečas, D. Choquesillo-Lazarte, P. V. Andreev and E. S. Shchegravina, *Polyhedron*, 2022, **228**, 116157.
41 Agilent, *CrysAlis PRO*, Agil. Technol. Ltd, Yarnton, Oxfordshire, UK, 2014.
42 G. M. Sheldrick, *Acta Crystallogr., Sect. A: Found. Adv.*, 2015, **71**, 3–8.
43 V. Petříček, L. Palatinus, J. Plášil and M. Dušek, *Z. Kristallogr. - Cryst. Mater.*, 2023, **238**, 271–282.
44 M. J. Frisch, *et al.*, *Gaussian 09, Revision A.02*, Gaussian Inc., Wallingford, CT, 2016.
45 P. R. Spackman, M. J. Turner, J. J. McKinnon, S. K. Wolff, D. J. Grimwood, D. Jayatilaka and M. A. Spackman, *J. Appl. Crystallogr.*, 2021, **54**, 1006–1011.
46 M. J. Turner, S. Grabowsky, D. Jayatilaka and M. A. Spackman, *J. Phys. Chem. Lett.*, 2014, **5**, 4249–4255.
47 M. A. Spackman, *CrystEngComm*, 2018, **20**, 5340–5347.
48 R. F. W. Bader, *Atoms in Molecules: A Quantum Theory*, Oxford University Press, Oxford, 1994.
49 T. Lu and F. Chen, *J. Comput. Chem.*, 2012, **33**, 580–592.
50 E. Espinosa, E. Molins and C. Lecomte, *Chem. Phys. Lett.*, 1998, **285**, 170–173.
51 M. A. Spackman, *Cryst. Growth Des.*, 2015, **15**, 5624–5628.
52 B. Bankiewicz, P. Matczak and M. Palusiak, *J. Phys. Chem. A*, 2012, **116**, 452–459.
53 U. Koch and P. L. A. Popelier, *J. Phys. Chem.*, 1995, **99**, 9747–9754.
54 M. G. Babashkina, D. A. Safin, M. Bolte, M. Srebro, M. Mitoraj, A. Uthe, A. Klein and M. Köckerling, *Dalton Trans.*, 2011, **40**, 3142–3153.
55 K. Metlushka, A. Tufatullin, L. Shaimardanova, D. Sadkova, K. Nikitina, O. Lodochnikova, O. Kataeva and V. Alfonsov, *Heteroat. Chem.*, 2014, **25**, 636–643.
56 M. C. Etter, J. C. MacDonald and J. Bernstein, *Acta Crystallogr., Sect. B: Struct. Sci.*, 1990, **46**, 256–262.
57 I. Rozas, I. Alkorta and J. Elguero, *J. Am. Chem. Soc.*, 2000, **122**, 11154–11161.
58 G. Rajput, V. Singh, A. N. Gupta, M. K. Yadav, V. Kumar, S. K. Singh, A. Prasad, M. G. B. Drew and N. Singh, *CrystEngComm*, 2013, **15**, 4676–4683.
59 M. P. Mitoraj, M. G. Babashkina, K. Robeyns, F. Sagan, D. W. Szczepanik, Y. V. Seredina, Y. Garcia and D. A. Safin, *Organometallics*, 2019, **38**, 1973–1981.
60 C. R. Groom, I. J. Bruno, M. P. Lightfoot and S. C. Ward, *Acta Crystallogr., Sect. B: Struct. Sci., Cryst. Eng. Mater.*, 2016, **72**, 171–179.